Communication

Impedance Coupled Voltage Boosting Circuit for Polyvinylidene Fluoride Based Energy Harvester

Kibae Lee [1], Yoonsang Jeong [1], Chong Hyun Lee [1,*], Jongkil Lee [2], Hee-Seon Seo [3] and Yohan Cho [3]

[1] Department of Ocean System Engineering, Jeju National University, Jeju 63243, Republic of Korea
[2] Department of Mechanical Engineering Education, Andong National University,
     Andong 36729, Republic of Korea
[3] Agency for Defense Development, Daejeon 34186, Republic of Korea
* Correspondence: chonglee@jejunu.ac.kr; Tel.: +82-64-754-3481

Abstract: Polyvinylidene fluoride (PVDF) is an emerging method for energy harvesting by fluid motion with superior flexibility. However, the PVDF energy harvester, which has a high internal impedance and generates a low voltage, has a large power transmission loss. To overcome this problem, we propose an impedance-coupled voltage-boosting circuit (IC-VBC) that reduces the impedance of the PVDF energy harvester and boosts the voltage. SPICE simulation results show that IC-VBC reduces the impedance of the PVDF energy harvester from 4.3 MΩ to 320 kΩ and increases the output voltage by 2.52 times. We successfully charged lithium-ion batteries using the PVDF energy harvester and IC-VBC with low-speed wind power generation.

Keywords: energy harvesting; polyvinylidene fluoride; impedance coupling; voltage boosting

1. Introduction

Recently, the demand for renewable energy and the internet of things (IoT) has increased and this has urged the development of independent energy production technology for wearable devices. For energy harvesting, research using piezoelectricity, thermoelectricity, and triboelectricity is being conducted [1–6]. Especially, Piezoelectric elements are emerging materials for miniaturized energy generation with small size and high energy efficiency [7–9]. Polyvinylidene fluoride (PVDF) has been studied because it can generate low-speed wind power with a small size compared to conventional wind power generators [10–16]. However, the PVDF, which has a high internal impedance with thin thickness and generates a low voltage, causes a large leakage of power [17].

A rectifier circuit using a bridge diode is mainly used to deliver AC power generated by piezoelectric elements [18,19]. However, the bridge diode rectifier circuit causes power loss due to the forward voltage drop of diodes.

To overcome this power loss, a voltage doubler rectifier circuit was used [20,21]. The voltage doubler rectifier circuit using two diodes and capacitors can double the voltage produced by piezoelectric elements. However, it can cause power loss in energy harvesting using PVDF because it increases the intrinsic impedance of the harvesting circuit.

A voltage multiplier circuit and voltage-controlled switch were used for efficient power transfer of the PVDF energy harvester [22]. This method has practical limitations in that power cannot be continuously transferred and additional power is consumed for switching operation. Impedance coupling methods using a switch have been proposed to transfer power from an energy source with high impedance [23–25]. However, these methods have limited use for high-voltage sources and consume additional power for switching operations. Liang et al. reduced the impedance of the energy source without additional power consumption using capacitors and MOSFET transistors, but it can be used limitedly in harvesters that generate high voltage [26]. A circuit using a transformer for impedance matching was proposed by Zhu et al. [27]. This circuit can only be used for

high input frequencies of several kHz and usually uses a large custom-made transformer of high inductance.

Cockcroft-Walton cascade voltage doubler circuit and Karthaus-Fischer cascade voltage doubler circuit were used for low-power energy harvesting circuits adopting Piezoelectric transducers [28]. Duque et al. proposed a voltage elevator circuit using two capacitors and an active rectifier circuit reducing forward voltage drop [29]. A charge pump rectifier circuit using many diodes and capacitors is used for low-power energy harvesting using photovoltaic cells, thermoelectric generators, etc. [30,31]. These methods increase the voltage efficiently by using multiple capacitors, but increase the impedance of the harvester and cause transmission loss of power.

To overcome this problem, we propose an impedance-coupled voltage-boosting circuit (IC-VBC) that reduces the impedance of the PVDF energy harvester and boosts the voltage. The proposed IC-VBC consists of a voltage-boosting stage that increases voltage and a storing stage that transfers power by coupling impedance. The voltage-boosting stage stores power in multiple capacitors connected in parallel and boosts the voltage by switching to a series connection. The storing stage implements a switch without power consumption by using MOSFET transistors and delivers power by matching the impedance to the electrical load. The proposed IC-VBC reduced the internal impedance of the PVDF energy harvester and increased the voltage to successfully generate low-speed wind power.

Our paper is organized as follows: Section 2 describes the IC-VBC. In Section 3, we design IC-VBC and describe the SPICE simulation results. In Section 4, the experimental results with low-speed wind generation are described and lithium-ion battery charging is demonstrated. Conclusions are presented in Section 5.

2. IC-VBC

Figure 1 shows the working principle of the proposed IC-VBC. The differential signal V_s generated by the PVDF energy harvester is stored in K capacitors C_k^P and C_k^N of the equal capacitance connected in parallel according to the current direction. Based on the clockwise current flow, C_k^P are charged while V_s is a positive voltage and C_k^N are charged while V_s is a negative voltage. The total capacitances of $C_{parallel}^P$ and $C_{parallel}^N$ of K parallel-connected capacitors are computed by K times as Equation (1).

$$C_{parallel}^{P,N} = \sum_k C_k^{P,N} = KC \tag{1}$$

where we assume that the capacitance of single capacitor $C_k^{P,N}$ is equal to C so that $C_k^{P,N} = C$, $k = 1, 2, \cdots, K$. The voltage charged to the K capacitors connected in parallel is expressed as a function of time as follows:

$$V_{charge}^{P,\,N}(t) = V_S \left(1 - e^{-\frac{t}{Z_0 KC}} \right) \tag{2}$$

where Z_0 is the internal impedance of the PVDF energy harvester. The electric charges charged in C_k^P and C_k^N are transferred to C_{store} by crossing two switches in the storing stage. At the same time, the switches located in the voltage boosting stage operate alternately according to the current direction. While C_k^P and C_k^N are charged, the switches are open and the K capacitors are connected in parallel. On the other hand, while C_k^P and C_k^N are discharged, the switches are closed and the K capacitors are connected in series. The total capacitances of C_{series}^P and C_{series}^N of K series-connected capacitors are computed as follows:

$$C_{series}^{P,N} = \left(\sum_k C_k^{P,N} \right)^{-1} = \frac{C}{K} \tag{3}$$
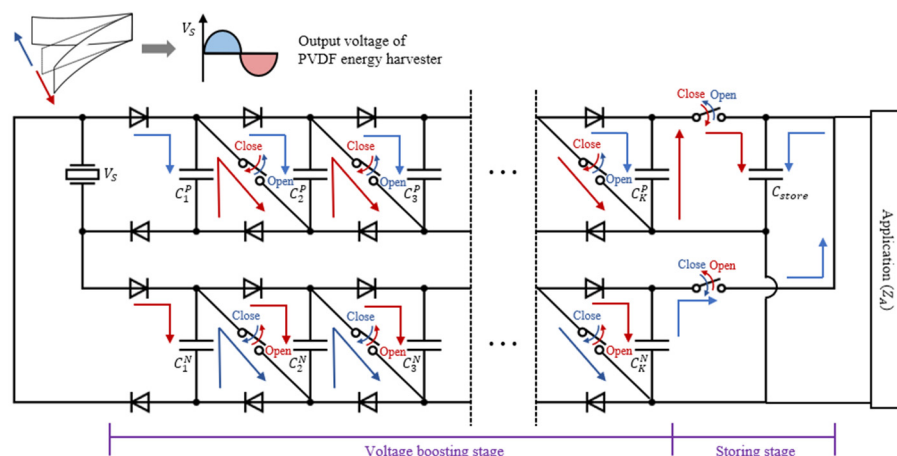
Figure 1. Working principle of IC-VBC.

The discharged voltage of the *K* capacitors connected in series is expressed as a function of times, as follows:

$$V_{discharge}^{P,N}(t) = KV_S \times e^{-\frac{t}{Z_L C/K}} \tag{4}$$

where Z_L is the load impedance of C_{store}. Therefore, the voltage is boosted *K* times while C_k^P and C_k^N are discharged, and the power can be transferred to C_{store} more quickly.

C_{store} in IC-VBC has a large capacitance to store a lot of energy. Therefore, Z_L is computed as the inverse function of C_{store} and has a low value. On the other hand, the PVDF energy harvester has a high internal impedance with a thin thickness. This impedance difference causes a large leakage in power transfer. The proposed IC-VBC delivers power to the load by reducing the impedance of the PVDF energy harvester via a cross-switching operation according to the current direction of V_s. The matched impedance Z_M is determined as in Equation (5) by the capacitance and number of capacitors constituting the voltage boosting stage.

$$Z_M = \frac{1}{2\pi f \frac{C}{K}} \tag{5}$$

where *f* is the fundamental frequency of V_s. The power stored in C_{store} is supplied to the electrical load Z_A to drive applications such as sensors and electronic devices. The cross-switching function of the IC-VBC is implemented using MOSFET transistors. Figure 2 shows the schematic circuit diagram of IC-VBC with $K = 3$.
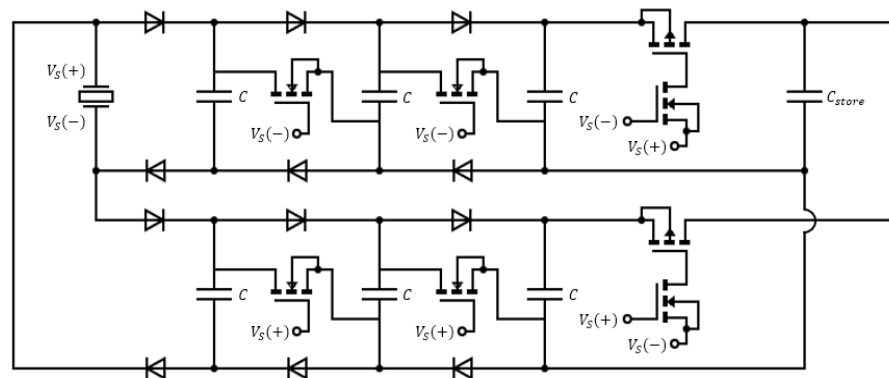

Figure 2. Circuit diagram of IC-VBC ($K = 3$).

Figure 3 shows the working flow chart of IC-VBC. The working flow of IC-VBC is as follows:

(1) At positive V_s, K capacitors of C_k^P are connected in parallel and the charged voltage is expressed as Equation (2).

(2) At negative V_s, the switches are closed and the K capacitors are connected in series. These series connection increasing voltage K times delivers the power to C_{store}. The charged voltage is expressed as Equation (4). Note that the switches are opened and the K capacitors C_k^N connected in parallel are charged with negative V_s at the same time.

(3) When V_s becomes positive again, the C_k^P are connected in parallel and charged, and the C_k^N are connected in series to deliver power to the C_{store}.
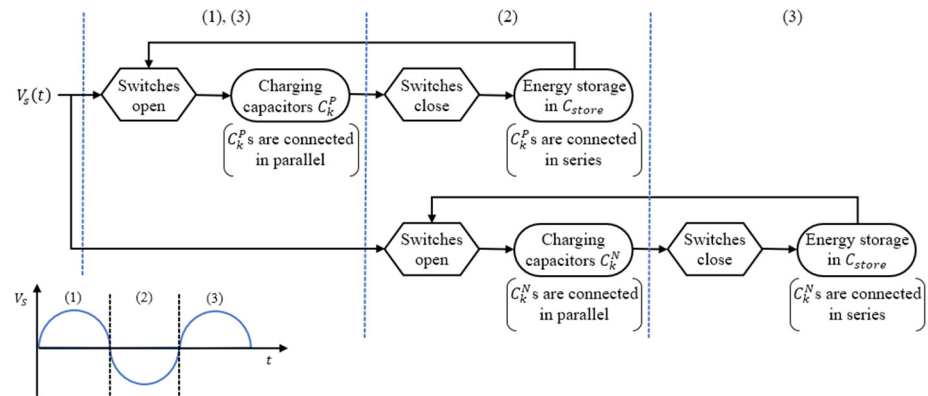

Figure 3. Working flow chart of IC-VBC.

3. Simulation Results

For SPICE simulation, we measure the generated voltage of the PVDF energy harvester according to wind power and estimate the source voltage. We measured the generated signals according to wind speeds of approximately 4 m/s, 6 m/s and 8 m/s using a PVDF energy harvester of 155.7 mm × 18.0 mm × 0.157 mm (height × width × thickness). Figure 4 shows the generated signal and frequency spectrum of the PVDF energy harvester measured at 10 MΩ with an oscilloscope (DSO7052B, Agilent Technologies, Santa Clara, CA, USA). The PVDF generates unstable velocity distribution by vortex flow and increases directional deformation proportional to fluid velocity [22]. Therefore the PVDF energy harvester generates a high voltage proportional to the wind speed and includes a fundamental frequency of 2.9 Hz to 3.7 Hz and frequency components of 12 Hz and 35 Hz.
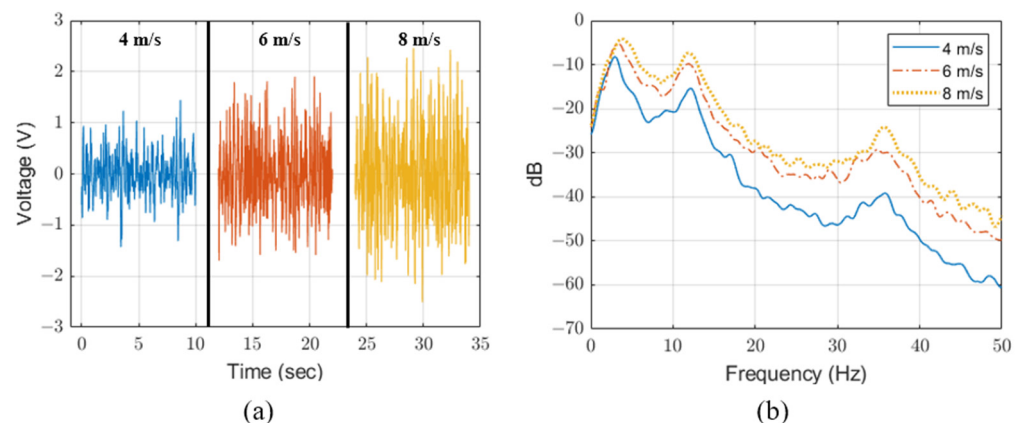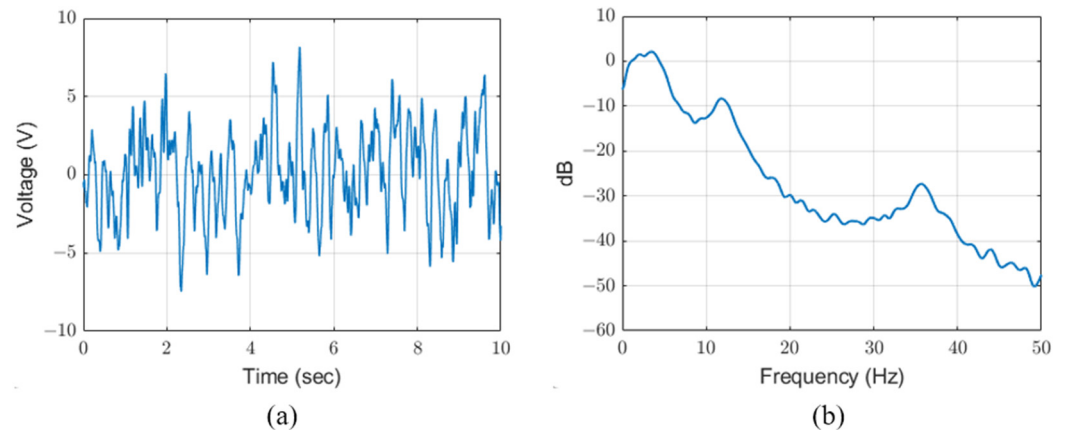

**Figure 4.** (**a**) Output voltage and (**b**) frequency spectrum of PVDF energy harvester.

The PVDF energy harvester is equivalent to a circuit model of internal capacitance C_0 and source voltage V_0, connected in series [22]. The determined internal capacitance using an LCR meter, C_0, is found to be 10.26 nF. The C_0 is similar to the nominal capacitance of 11 nF of the used PVDF (LDT1-028K, TE Connectivity, Schaffhausen, Switzerland). The

source voltage, V_0, can be estimated using a first-order Butterworth inverse filter at the measured voltage at 10 MΩ [22]. Figure 5 shows the estimated source using the measured voltage at 8 m/s wind speed. In Figure 5b, the fundamental frequency of 3.7 Hz has a large difference of more than 10 dB compared to the frequencies of 11 Hz and 35 Hz. The internal impedance of the PVDF energy harvester is calculated and found to be $1/2\pi f C_0 = 4.19$ MΩ with $f = 3.7$ Hz.
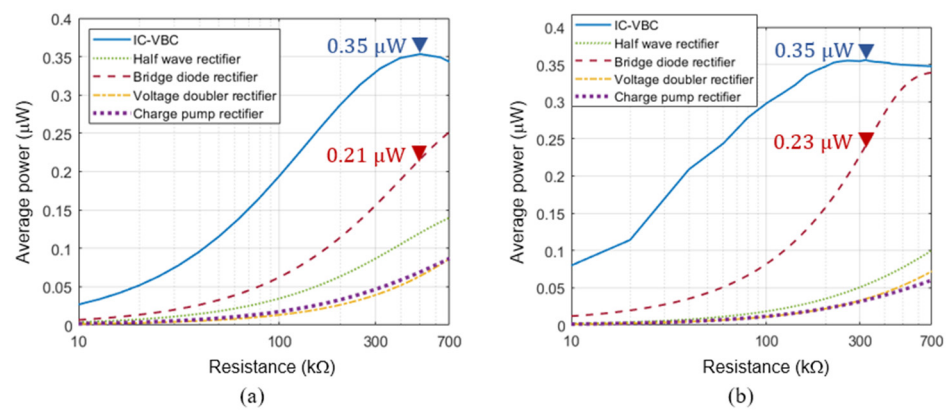

Figure 5. (**a**) Estimated source voltage and (**b**) frequency spectrum of PVDF energy harvester at 8 m/s wind speed.

Conventional bridge diode rectifier circuits, voltage doubler rectifiers, and charge pump rectifier circuits are used for energy harvesting [22,32,33]. Half wave rectifier, bridge diode rectifier, voltage doubler, and charge pump rectifier circuits were considered as shown in Figure 6 and their average powers according to load were compared with the IC-VBC via SPICE simulation. For simulation, we set $K = 2$, $C = 170$ nF so that $Z_m = 500$ kΩ in Equation (5) and implemented the IC-VBC using Infineon's BSP92P and IRL510 MOSFET transistors and Vishay's BAT43 diode. The comparison results are shown in Figure 7 by using the same Vishay's BAT43 diode for all rectifier circuits.
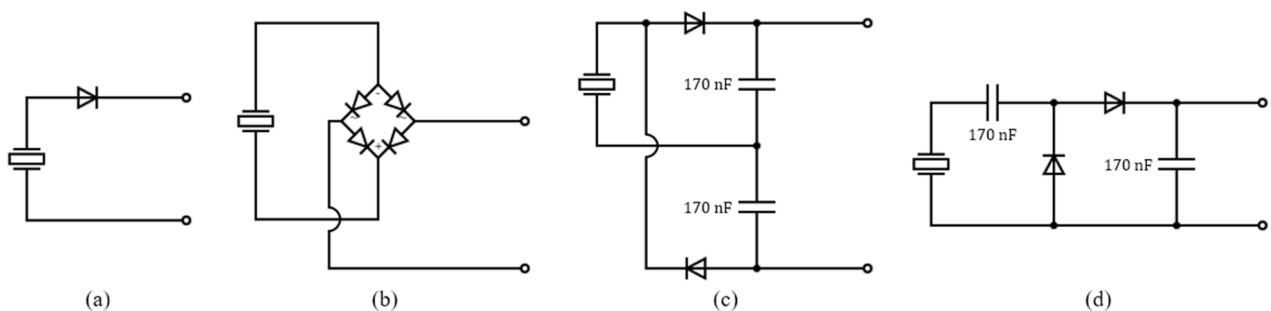
Figure 6. (**a**) Half wave rectifier, (**b**) bridge diode rectifier, (**c**) voltage doubler rectifier and (**d**) charge pump rectifier circuit.

Figure 7a shows the results obtained by using a source voltage of 3.7 Hz and assuming constant directional deformation of PVDF over time. The proposed IC-VBC can match the 500 kΩ impedance of the PVDF and supply 1.6 times higher power than the bridge diode rectifier circuit. Figure 7b showing the simulation with source voltage estimated from measured data, shows that the IC-VBC reduces the impedance of the PVDF from 4.19 MΩ to 320 kΩ and supplies 1.52 times higher power than the bridge diode rectifier circuit.

Figure 7. Comparison of average power between IC-VBC and conventional rectifier circuits using (**a**) simulated source voltage and (**b**) estimated source voltage from experimental data.

The voltage multiplier circuits such as the voltage doubler rectifier and the charge pump rectifier use two capacitors in series for voltage boosting. The connected capacitors inevitably increase the impedance of the PVDF energy harvester and cause power transfer loss. Therefore, the voltage multiplier circuits supply lower power than the IC-VBC and the bridge diode rectifier circuit.

We set $C_{store} = 10\ \mu F$ for various applications as described in Appendix B and compared the charged voltage according to the number of capacitors in the voltage boosting stage and wind speed. As described in Appendix A, C is set differently depending on the number of capacitors so that $Z_m = 500\ k\Omega$ in Equation (5). Figure 8a shows the charged voltage in C_{store} according to the number of capacitors in the voltage-boosting stage. The charged voltage is 1.49 V when a single capacitor is used in the voltage boosting stage. The voltage is boosted 1.95 times to charge 2.90 V when two capacitors are used and boosted 2.52 times to charge 3.75 V when three capacitors are used. Conventionally, passive devices can have a characteristic error within ±15% [34,35]. The characteristic error of the internal resistance of the diodes and capacitors in the IC-VBC causes a deviation of the voltage charged in C_{store}. Therefore, the voltage charged in C_{store} may have a deviation of 1.12 V due to the characteristic error of the passive devices when three capacitors are used. Figure 8b shows the voltage charged in C_{store} according to the wind speed. Three capacitors were used in the voltage-boosting stage of the IC-VBC. The charged voltage is 1.98 V when the wind speed is 4 ms, and we can charge approximately 0.9 V elevated voltage when the wind speed increases by 2 m/s.
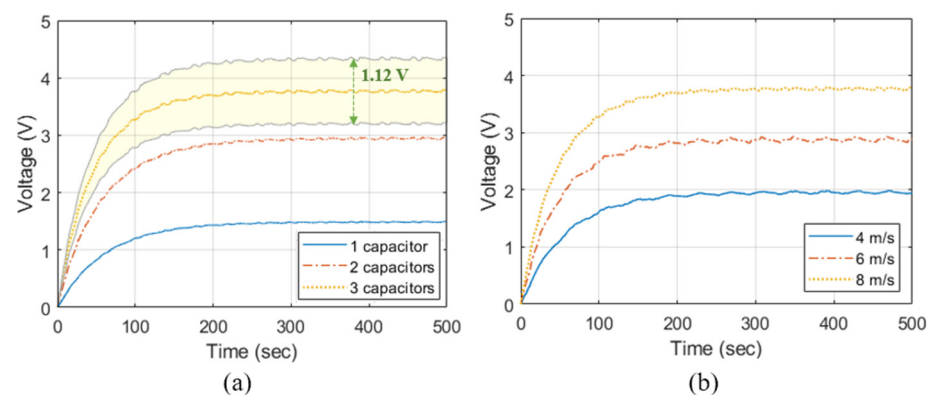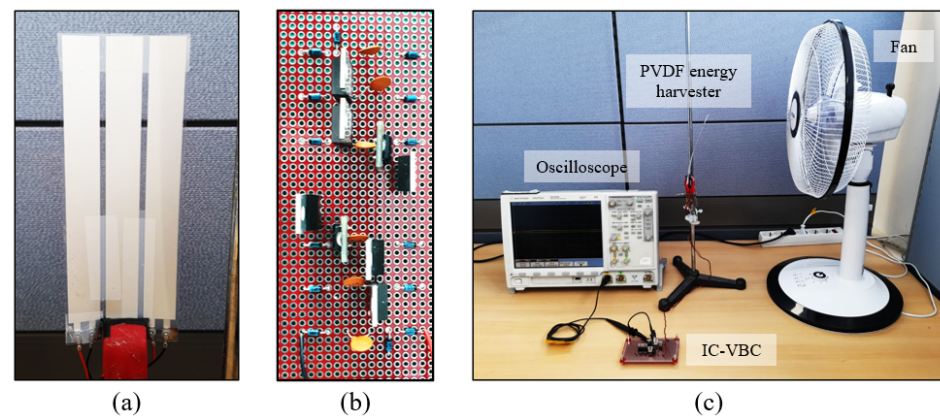

Figure 8. Charged voltage according to (**a**) number of capacitors at 8 m/s wind speed and (**b**) wind speed with 3 capacitors.

4. Experiment Results

We implemented IC-VBC connected to the PVDF energy harvester and verified the integrated system through experiments as sown in Figure 9. The PVDF energy harvester

and the IC-VBC was implemented identically to the SPICE simulation. Figure 10 shows the charged into C_{store}, which is obtained by an average of 10 experiments by changing the number of capacitors and PVDFs. Figure 10a shows the voltage charged in C_{store} according to the number of capacitors at a wind speed of approximately 8 m/s. The charged voltages are 1.43 V and 2.68 V when a single and two capacitors are used in the voltage boosting stage. The charged voltage is 3.38 V, which is 2.36 times higher than when a single capacitor is used, or when three capacitors are used. These results are within the range of deviation due to a characteristic error of $\pm 15\%$ in the SPICE simulation. The voltage charged in C_{store} reaches the maximum voltage after approximately 600 s regardless of the number of capacitors in the voltage boosting stage.

Figure 9. (**a**) PVDF energy harvester, (**b**) IC-VBC, (**c**) experimental setup.
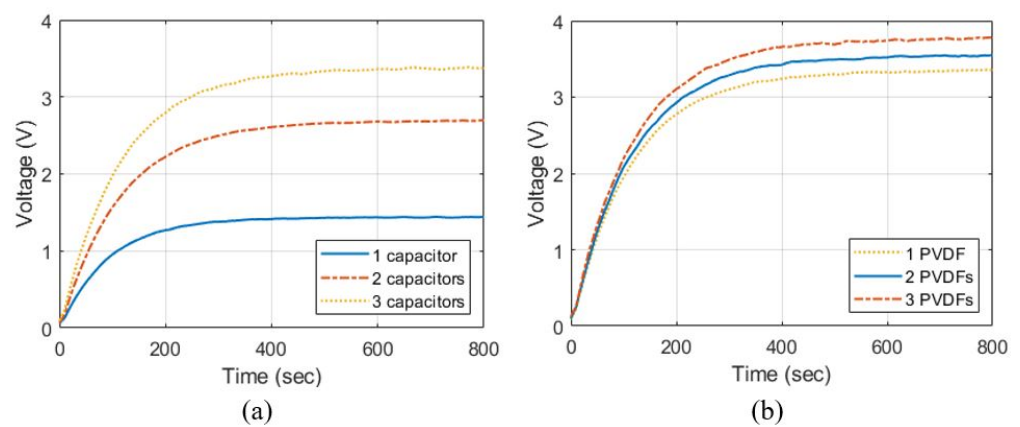

Figure 10. Charged voltage according to (**a**) number of capacitors with single PVDF at 8 m/s wind speed and (**b**) number of PVDFs with 3 capacitors at 8 m/s wind speed.

Multiple PVDFs were attached as shown in Figure 9a and connected in series to the IC-VBC. Figure 10b shows the voltage charged in C_{store} according to the number of PVDFs. We used three capacitors in the voltage boosting stage of IC-VBC and measured the voltage at a wind speed of approximately 8 m/s. Subsequently, we can charge a voltage of 3.73 V using three PVDF energy harvesters.

For a practical application of the suggested IC-VBC, we demonstrated the charging of a conventional lithium-ion battery. We charged Seiko's MS621FE lithium-ion battery using the IC-VBC which includes the voltage boosting stage with three capacitors and three PVDFs generating a voltage of 3.73 V as shown in Figure 10b. The MS621FE lithium-ion battery is charged using a voltage of 2.85 V to 3.8 V [36]. We use Analog's ADP5304 switch to transfer power from IC-VBC to a lithium-ion battery [37]. Figure 11a shows the output voltage of the IC-VBC and the current transferred to the lithium-ion battery. A power of 304 μW is transferred to the lithium-ion battery when the output voltage of the IC-VBC

reaches 3.8 V. The battery charging system implemented with the PVDF energy harvester and the IC-VBC has a power transfer cycle of approximately 58 s.
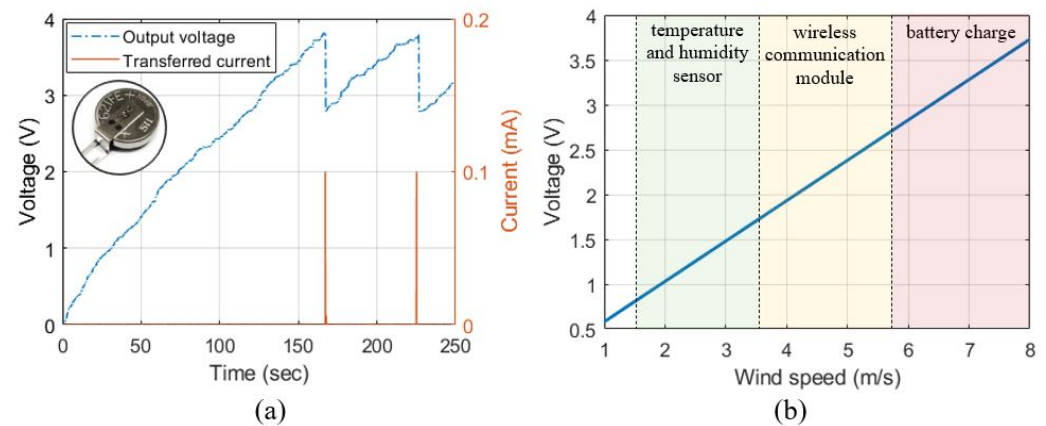
Figure 11. (**a**) Output voltage of IC-VBC and current transferred to lithium-ion battery, (**b**) estimated output voltage of IC-VBC according to wind speed.

As described in Section 2, the voltage charged in C_{store} increases by 0.9 V as the wind speed increases by 2 m/s. Therefore, the output voltage of IC-VBC, which uses three PVDFs and three capacitors in the voltage boosting stage, according to the wind speed is estimated as Equation (6) based on the output voltage of 3.73 V at 8 m/s wind speed as described in Appendix C.

$$V_{out}(s) = 3.73 - 0.45(8 - s) \tag{6}$$

where s is wind speed. Figure 11b shows the output voltage of IC-VBC according to the wind speed and the applications that can be utilized. The lithium-ion battery can be charged at a wind speed of approximately 5.9 m/s or higher, as shown in the previous experimental results. We can generate a 1.8 V driving voltage for a wireless communication module for IoT applications at wind speeds over 3.7 m/s [38]. In addition, we can drive temperature and humidity determination sensors capable of low voltage operation with low-speed wind power generation of 3.7 m/s or less [39,40].

5. Conclusions

We propose the IC-VBC for efficient power transfer of the PVDF energy harvester with high internal impedance and low voltage output. The proposed IC-VBC consists of the voltage boosting stage with multiple capacitors and the storing stage that delivers power to the electrical load. Capacitors of the voltage boosting stage are connected in parallel to the charge, and are connected in series via MOSFET switching to transfer power. Capacitors connected in series transfer power efficiently by boosting the voltage and reducing the total capacitance. The MOSFET transistors in storing stage automatically couple the impedance between the PVDF energy harvester and the electrical load. Therefore, the IC-VBC can reduce the impedance of the PVDF energy harvester during the power transfer process. SPICE simulation results show that IC-VBC reduces the impedance of the PVDF energy harvester from 4.3 MΩ to 320 kΩ and increases the output voltage by 2.52 times. We successfully charged lithium-ion batteries using the PVDF energy harvester and IC-VBC with low-speed wind power generation.

Appendix A. Determination of the Number of Capacitors and Capacitance

The capacitors of C_k^N, C_k^P in IC-VBC can reduce overall impedance including the PVDF and IC-VBC. The overall impedance Z_M reduced by the IC-VBC can be computed with Equation (5). By setting $Z_M = 500$ kΩ and $f = 3.7$ Hz, we can determine the capacitance C with K capacitors as follows:

$$\frac{C}{K} = \frac{1}{2\pi f Z_m} = \frac{1}{2\pi \times 3.7 \times (500 \times 10^3)} = 85 \times 10^{-9} \tag{A1}$$

we can reduce internal impedance from 4.19 MΩ to 320 kΩ as shown in Table A1.

Table A1. Capacitance C set according to the number of capacitors K.

The Number of Capacitors (K)	Capacitance (C)	Matched Impedance (Z_M) in SPICE Simulation
1	82 nF	320 kΩ
2	170 nF	320 kΩ
3	255 nF	320 kΩ

The K capacitors connected in parallel at the voltage boosting stage are converted into a series connection by cross-switching and then their power is transferred to C_{store}. This series capacitor connection increases total voltage K times as expressed in Equation (4).

The magnitude of the voltage, however, is limited by the input power. The power transfer model of the IC-VBC proposed is equivalent as shown in Figure A1. The input power P_{in} to the IC-VBC can be computed by input voltage V_S and input impedance Z_{in} of the voltage boosting stage and can be described as follows:

$$P_{in} = \frac{V_S^2}{Z_{in}} \tag{A2}$$

where Z_{in} can be computed by capacitance C and fundamental frequency f of V_S, i.e.,

$$Z_{in} = \frac{1}{2\pi f C} \tag{A3}$$

With boosted voltage KV_S and load impedance Z_L, the output power P_{out} delivered to C_{store} can be described as.

$$P_{out} = \frac{(KV_S)^2}{Z_L} \tag{A4}$$

where Z_L can be computed as follows:

$$Z_L = \frac{1}{2\pi f C_{store}} \tag{A5}$$

Since $P_{out} < P_{in}$, the following relationship can be derived

$$K < \frac{Z_M + Z_L}{\sqrt{Z_{in} Z_L}} \tag{A6}$$

We set $C = 85$ nF, $C_{store} = 10$ μF and $Z_M = 320$ kΩ and obtain optimum $K = 3$ via SPICE simulations.
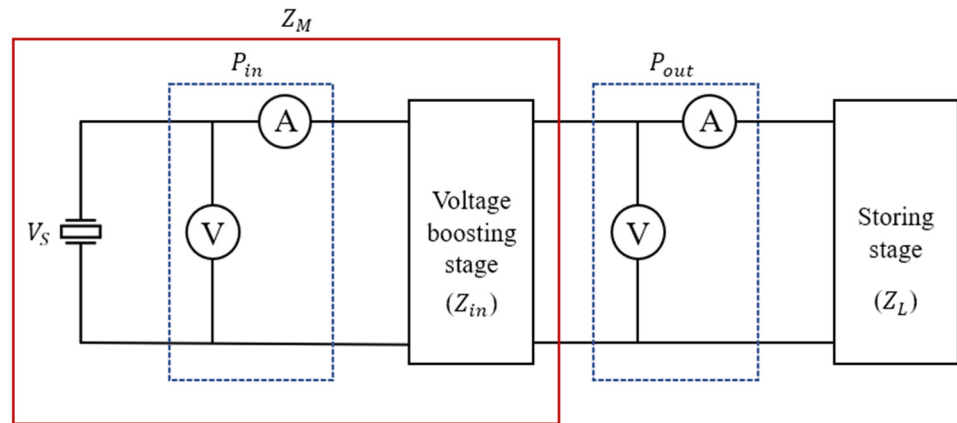
Figure A1. Power transfer model of IC-VBC.

Appendix B. Impedance Model for Applications

By SPICE simulations of IC-VBC for charging and electronic device, Z_M of 320 kΩ is obtained. Also, it is obtained that the Z_M matched PVDF energy harvester can deliver high power loads ranging from 230 kΩ to 420 kΩ with a deviation of 3.8 nW.

The impedance model of the IC-VBC including the electrical load can be depicted equivalently as shown in Figure A2. Here, Z_L is the load impedance of C_{store} and Z_A is the electrical load. Since Z_M and Z_L are connected in parallel, equivalent load Z_H can be written as follows:

$$Z_H = \frac{Z_M Z_L}{Z_M + Z_L} \tag{A7}$$

We set $C_{store} = 10$ μF because C_{store} should be much bigger than C/K for energy transfer using multiple capacitors [26], i.e., $C_{store} \gg C/K$. Then Z_H becomes 4.24 kΩ with $Z_L = 4.3$ kΩ and $f = 3.7$ Hz.
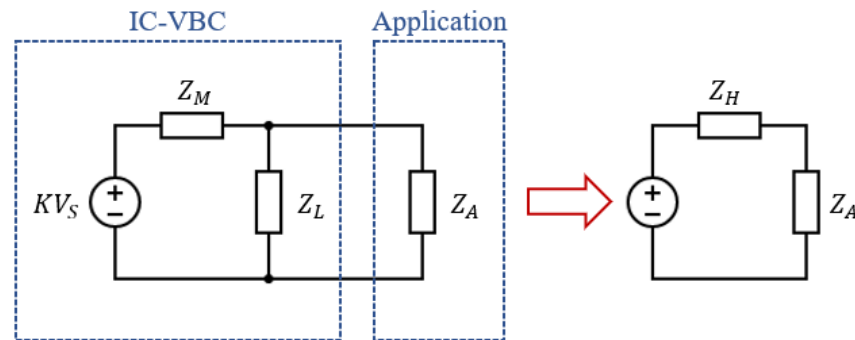

Figure A2. Equivalent impedance model of IC-VBC.

In this paper, we consider Seiko's MS621F lithium-ion battery [36] charging and implement the IC-VBC with Analog's ADP5304 switch [41]. Since the integrated impedance of the switch and the battery is 4.25 kΩ, the IC-VBC can efficiently transfer power. Note that the application of the IC-VBC is not limited as long as the electrical load is approximately 4 kΩ so that charging pressure and temperature sensors [42–44] become feasible applications of the IC-VBC.

Appendix C. Output Voltage of IC-VBC

The output voltage V_{out} obtained using the PVDF and the IC-VBC as a function of the wind speed s can be expressed as follows:

$$V_{out}(s) = V_{max} - V_{inc}(s_{max} - s) \tag{A8}$$

where V_{max} is the maximum voltage with maximum wind speed s_{max} and V_{inc} is increased voltage with a 1 m/s wind speed increment.

From the experimental results in Figure 10, we set s_{max} and V_{max} as 8 m/s and 3.73 V, respectively. Then the equation above can be written as follows:

$$V_{out}(s) = 3.73 - V_{inc}(8 - s) \tag{A9}$$

We obtain $V_{inc} = 0.9/2 = 4.5$ by using the results in Figure 8b which shows that output voltage increases by 0.9 V with a 2 m/s speed increment. Consequently, the output voltage can be written as follows:

$$V_{out}(s) = 3.73 - \frac{0.9}{2}(8 - s) = 3.73 - 0.45(8 - s) \tag{A10}$$

References

1. Song, R.; Shan, X.; Lv, F.; Xie, T. A study of vortex-induced energy harvesting from water using PZT piezoelectric cantilever with cylindrical extension. *Ceram. Int.* **2015**, *41*, S768–S773. [CrossRef]
2. Mehmood, A.; Abdelkefi, A.; Hajj, M.; Nayfeh, A.; Akhtar, I.; Nuhait, A. Piezoelectric energy harvesting from vortex-induced vibrations of circular cylinder. *J. Sound Vib.* **2013**, *332*, 4656–4667. [CrossRef]
3. Dai, H.; Abdelkefi, A.; Wang, L. Theoretical modeling and nonlinear analysis of piezoelectric energy harvesting from vortex-induced vibrations. *J. Intell. Mater. Syst. Struct.* **2014**, *14*, 1861–1874. [CrossRef]
4. Nechibvute, A.; Chawanda, A.; Luhanga, P. Piezoelectric energy harvesting devices: An alternative energy source for wireless sensors. *Smart Mater. Res.* **2012**, *2012*, 853481. [CrossRef]
5. Akaydin, H.D.; Elvin, N.; Andreopoulos, Y. Energy harvesting from highly unsteady fluid flows using piezoelectric materials. *J. Intell. Mater. Syst. Struct.* **2010**, *21*, 1263. [CrossRef]
6. Erturk, A.; Delporte, G. Underwater Thrust and Power Generation Using Flexible Piezoelectric Composites: An Experimental Investigation toward Self-powered Swimmer-sensor Platforms. *Smart Mater. Struct.* **2011**, *20*, 125013. [CrossRef]
7. Erturk, A.; Inman, D. *Piezoelectric Energy Harvesting*; John Wiley & Sons, Ltd.: West Sussex, UK, 2011; pp. 1–73.
8. Kim, H.S.; Kim, J.-H.; Kim, J.H. A review of piezoelectric energy harvesting based on vibration. *Int. J. Precis. Eng. Manuf.* **2011**, *12*, 1129–1141. [CrossRef]
9. Kim, H.W.; Batra, A.; Priya, S.; Uchino, K.; Markley, D.; Newnham, R.E.; Hofmann, H.F. Energy harvesting using a piezoelectric "Cymbal" transducer in dynamic environment. *Jpn. J. Appl. Phys.* **2004**, *43*, 6178. [CrossRef]
10. Taylor, G.W.; Burns, J.R.; Kammann, S.M.; Powers, W.B.; Welsh, T.R. The energy harvesting eel: A small subsurface ocean/river power generator. *IEEE J. Ocean. Eng.* **2001**, *26*, 539–547. [CrossRef]
11. Akaydin, H.D.; Elvin, N. Andreopoulous, Y. The performance of a self-excited fludic energy harvester. *Smart Mater. Struct.* **2012**, *21*, 025007. [CrossRef]
12. Nguyen, H.D.T.; Phan, H.T.; Wang, D.A. A miniature pneumatic energy generator using Kármán vortex street. *J. Wind. Eng. Ind. Aerodyn.* **2013**, *116*, 40–48. [CrossRef]
13. Li, S.; Yuan, J.; Lipson, H. Ambient wind energy harvesting using cross-flow fluttering. *J. Appl. Phys.* **2011**, *109*, 026104. [CrossRef]
14. Zhang, J.; Fang, Z.; Shu, C.; Zhang, J.; Zhang, Q.; Li, C. A rotational piezoelectric energy harvester for efficient wind energy haravesting. *Sens. Actuaors A Phys.* **2017**, *262*, 123–129. [CrossRef]
15. Alam, M.M.; Ghosh, S.K.; Sultana, A.; Mandal, D. An effective wind energy harvester of paper Ahs-mediated rapidly synthesized ZnO nanoparticle-interfaced electrospun PVDF fiber. *ACS Sustain. Chem. Eng.* **2018**, *6*, 292–299. [CrossRef]
16. Lu, L.; Ding, W.; Liu, J.; Yang, B. Flexible PVDF based piezoelectric nanogenerators. *Nano Energy* **2020**, *78*, 105251. [CrossRef]
17. Singh, H.H.; Sharma, H.B. Impedance spectroscopy and transport properties of polymer-based flexible nanocomposites. *Solid State Commun.* **2020**, *319*, 114012. [CrossRef]
18. Ottman, G.K.; Hofmann, H.F.; Bhatt, A.C.; Lesieutre, G.A. Adaptive piezoelectric energy harvesting circuit for wireless remote power supply. *IEEE Trans. Power Electron.* **2002**, *17*, 669–676. [CrossRef]
19. Zhao, J.; You, Z. A shoe-embedded piezoelectric energy harvester for wearable sensors. *Sensors* **2014**, *14*, 12497–12510. [CrossRef]
20. Tabesh, A.; Fréchette, L.G. A low-power stand-alone adaptive circuit for harvesting energy from a piezoelectric micropower generator. *IEEE Trans. Ind. Electron.* **2009**, *57*, 840–849. [CrossRef]
21. Kushino, Y.; Koizumi, H. Piezoelectric energy harvesting circuit using full-wave voltage doubler rectifier and switched inductor. In Proceedings of the 2014 IEEE Energy Conversion Congress and Exposition (ECCE), Pittsburgh, PA, USA, 14–18 September 2014; pp. 2310–2315.
22. Lee, J.; Ahn, J.; Jin, H.; Lee, C.H.; Jeong, Y.; Lee, K.; Seo, H.S.; Cho, Y. A funnel type PVDF underwater energy harvester with spiral structure mounted on the harvester support. *Micromachines* **2022**, *13*, 579. [CrossRef]
23. Xi, F.; Pang, Y.; Li, W.; Jiang, T.; Zhang, L.; Guo, T.; Liu, G.; Zhang, C.; Wang, Z.L. Universal power management strategy for triboelectric nanogenerator. *Nano Energy* **2017**, *37*, 168–176. [CrossRef]

24. Niu, S.; Wang, X.; Yi, F.; Zhou, Y.S.; Wang, Z.L. A universal self-charging system driven by random biomechanical energy for sustainable operation of mobile electronics. *Nat. Commun.* **2015**, *6*, 8975. [CrossRef] [PubMed]
25. Harmon, W.; Bamgboje, D.; Guo, H.; Hu, T.; Wang, Z.L. Self-driven power management system for triboelectric nanogenerators. *Nano Energy* **2020**, *71*, 104642. [CrossRef]
26. Liang, X.; Jiang, T.; Feng, Y.; Lu, P.; An, J.; Wang, Z.L. Triboelectric nanogenerator network integrated with charge excitation circuit for effective water wave energy harvesting. *Adv. Energy Mater.* **2020**, *10*, 2002123. [CrossRef]
27. Zhu, G.; Chen, J.; Zhang, T.; Jing, Q.; Wang, Z.L. Radial-arrayed rotary electrification for high performance triboelectric generator. *Nat. Commun.* **2014**, *5*, 3426. [CrossRef] [PubMed]
28. Abidn, N.A.K.Z.; Nayan, N.M.; Azizan, M.M.; Ali, A. Analysis of voltage multiplier circuit simulation for rain energy harvesting using circular piezoelectric. *Mech. Syst. Signal Process.* **2018**, *101*, 211–218. [CrossRef]
29. Duque, M.; Leon-Salguero, E.; Sacristan, J.; Esteve, J.; Murillo, G. Optimization of a piezoelectric energy harvester and design of a charge pump converter for CMOS-MEMS monolithic integration. *Sensors* **2019**, *19*, 1895. [CrossRef]
30. Ballo, A.; Grasso, A.D.; Palumbo, G. A review of charge pump topologies for the power management of IoT nodes. *Electronics* **2019**, *8*, 480. [CrossRef]
31. Kawauchi, H.; Tanzawa, T. A fully integrated clocked AC-DC charge pump for mignetostrictive vibration energy harvesting. *Electronics* **2020**, *9*, 2194. [CrossRef]
32. Jabbar, H.; Song, Y.S.; Jeong, T.T. RF energy harvesting system and circuits for charging of mobile devices. *IEEE Trans. Consum. Electron.* **2010**, *56*, 247–253. [CrossRef]
33. Peng, H.; Tang, N.; Yang, Y.; Heo, D. CMOS startup charge pump with body bias and backward control for energy harvesting step-up converters. *IEEE Trans. Circuits Syst. I Regul. Pap.* **2014**, *61*, 1618–1628. [CrossRef]
34. High Voltage Products, Radial Leaded Capacitors. Available online: http://hvp.kr/sub/sub02_01.php?mode=list&cat_no=93 (accessed on 7 January 2013).
35. SAMSUNG Electro-Mechanics. Multilayer Ceramic Capacitors. Available online: https://www.samsungsem.com/global/product/passive-component/mlcc.do (accessed on 25 July 2022).
36. Seiko Instruments Inc. MS621FE. Available online: https://www.sii.co.jp/en/me/datasheets/ms-rechargeable/ms621fe/ (accessed on 1 February 2014).
37. Ahn, J.; Kim, J.S.; Jeong, Y.; Hwang, S.; Yoo, H.; Jeong, Y.; Gu, J.; Mahato, M.; Ko, J.; Jeon, S.; et al. All-recyclable triboelectric nanogenerator for sustainable ocean monitoring systems. *Adv. Energy Mater.* **2022**, *12*, 2201341. [CrossRef]
38. Microchip. WLR089U0. Available online: https://www.microhip.com/en-us/product/WLR089U0 (accessed on 6 January 2022).
39. ASAIR. HDS10. Available online: http://www.aosong.com/en/products-109.html (accessed on 17 October 2022).
40. NXP. PC2202. Available online: https://www.nxp.com/products/sensors/ic-digital-temperature-sensors/ultra-low-power-1-8-v-1-deg-c-accuracy-digital-temperature-sensor-with-ic-bus-interface:PCT2202UK (accessed on 14 August 2015).
41. Analog Devices. ADP5304. Available online: https://www.analog.com/en/products/adp5304.html (accessed on 11 February 2015).
42. Texas Instruments. XTR101. Available online: https://www.ti.com/product/XTR101 (accessed on 3 August 2004).
43. Honeywell. 500 Series. Available online: https://sps.honeywell.com/kr/ko/products/advanced-sensing-technologies/industrial-sensing/industrial-sensors/temperature-sensors/temperature-probes/500-series (accessed on 14 September 2021).
44. Futurlec. NTC4K. Available online: https://www.futurlec.com/Components_Others/NTC4Kpr.shtml (accessed on 1 January 2022).